PROCEEDINGS OF SCIENCE

Multimessenger emission from winds and tori in active galactic nuclei

Susumu Inoue,[a,b,c,*] **Matteo Cerruti,**[d,e] **Kohta Murase**[f,g,h] **and Ruo-Yu Liu**[i]

[a] *Theoretical Astrophysics Group, Tokyo Metropolitan University, Hachioji, Japan*
[b] *Faculty of Education, Bunkyo University, Koshigaya, Japan*
[c] *Astrophysical Big Bang Laboratory and iTHEMS, RIKEN, Wako, Japan*
[d] *Université Paris Cité, CNRS, Astroparticule et Cosmologie, F-75013 Paris, France*
[e] *Universitat de Barcelona, ICCUB, IEEC-UB, E-08028 Barcelona, Spain*
[f] *Department of Physics; Department of Astronomy & Astrophysics, Center for Multimessenger Astrophysics of Institute for Gravitation and the Cosmos, Penn State University, University Park, USA*
[g] *School of Natural Sciences, Institute for Advanced Study, Princeton, New Jersey, USA*
[h] *Yukawa Institute of Theoretical Physics, Kyoto University, Kyoto, Japan*
[i] *Nanjing University, Nanjing, China*

E-mail: sinoue@tmu.ac.jp

Powerful winds with wide opening angles, likely driven by accretion disks around black holes (BHs), are observed in the majority of active galactic nuclei (AGN) and can play a crucial role in AGN and galaxy evolution. If protons are accelerated in the wind near the BH via diffusive shock acceleration, pp as well as $p\gamma$ processes generate neutrinos together with pair cascade emission from the gamma-ray to radio bands. The TeV neutrinos detected by IceCube from the obscured Seyfert galaxy NGC 1068 may arise from optically thin, collisionless shocks in a failed, line-driven wind that is physically well motivated. Although the cascade emission is $\gamma\gamma$-attenuated above a few MeV, it can still contribute significantly to the sub-GeV gamma rays observed from NGC 1068, and possibly also its sub-millimeter emission. At higher energies, gamma rays can occur via pp processes from a shock where an outgoing wind impacts the obscuring torus, along with some observable GHz-band emission. Tests and implications of this model are discussed. Neutrinos and gamma rays may offer unique probes of AGN wind launching sites, particularly for objects obscured in other forms of radiation. This article includes updates to the work of Ref. [1].

38th International Cosmic Ray Conference (ICRC2023)
26 July - 3 August, 2023
Nagoya, Japan

ICRC2023
38th International Cosmic Ray Conference
The Astroparticle Physics Conference

*Speaker

PoS(ICRC2023)1161

1. Introduction

Active galactic nuclei (AGN) are likely powered mainly by accretion disks around supermassive black holes (BHs). Less than 10% of all AGN in the present Universe are of the radio-loud class that produce powerful, collimated jets of plasma with ultra-relativistic outflow velocities [2]. The majority of AGN are instead classified as radio-quiet and do not possess prominent jets. Nonetheless, there is widespread evidence that most AGN can eject winds of thermal plasma with wide opening angles ($2\theta_w \gtrsim$ 60-100 deg) and a range of outflow velocities ($v_w \sim$ few 100 km/s - $0.4c$), observable as blue-shifted atomic absorption features in the ultraviolet (UV) to X-ray bands [3, 4]. The fastest winds in X-rays are known as ultrafast outflows (UFOs) and seen in $\gtrsim$40% of all nearby AGN, of both radio-loud and radio-quiet types. Inferred to occur on sub-pc scales, their kinetic power can reach a substantial fraction ($L_w \lesssim$ 20-40%) of the bolometric luminosity $L_{\rm bol}$. In relatively nearby AGN, winds can also be discerned in the kinematics of their narrow emission line regions (NLR) on sub-kpc scales [3].

Such AGN-driven winds may be launched from accretion disks by mechanisms involving radiative and/or magnetic processes [4]. Winds are potentially ubiquitous in AGN with sufficiently high Eddington parameter $\lambda_{\rm Edd}$ (ratio of AGN bolometric luminosity $L_{\rm bol}$ to Eddington luminosity). AGN winds may play crucial roles in the collimation of jets in radio-loud AGN [2], as well as in the evolution of supermassive BHs and their host galaxies through their feedback effects onto their environment [5].

The kinetic energy of AGN winds may be partly dissipated and channelled into high-energy electrons and protons via mechanisms such as diffusive shock acceleration (DSA) [6]. This can induce non-thermal emission, e.g. from external shocks where the wind interacts with the host galaxy gas [8, 9]. Despite some tentative evidence [7], such emission is yet to be clearly discerned.

Also likely generic to all relatively luminous AGN is a geometrically thick torus of dusty, clumpy gas surrounding the nucleus on pc scales [10]. Depending on its inclination relative to the observer, such tori can substantially absorb the optical to X-ray emission from the accretion disk, resulting in the known differences between type-1 (unobscured) and type-2 (obscured) AGN. The absorbed energy is reprocessed into the observed infrared (IR) emission.

NGC 1068, an archetypal type-2 Seyfert galaxy at distance $D \sim$10-16 Mpc, is a known source of GeV gamma rays [11] as well as TeV neutrinos [12]. Although UV-X-ray signatures of winds on sub-pc scales are unobservable due to high obscuration by its torus [13], its NLR on larger scales exhibit an outflow with $v_{w,\rm NLR} \lesssim 2000$ km/s and $L_{w,\rm NLR} \lesssim 10^{43}$ erg/s, likely driven by the accretion disk [17]. The nature of the gamma rays detected by Fermi-LAT at energies $E_\gamma \sim 0.1 - 20$ GeV [11] is unclear, exceeding the inferred level associated with star formation in the host galaxy (i.e. pp π^0-decay gamma rays from interaction of cosmic rays from supernovae and interstellar gas) [14, 15].

Neutrino observations by IceCube [12] reveal that the most significant position in the northern hemisphere in a full-sky scan is coincident with that of NGC 1068. Independently, a 4.2σ excess over background expectations is found at its position in a source catalog search. The spectrum is quite soft, with muon neutrino flux best fit as $f_{\nu_\mu} \propto \varepsilon_\nu^{-3.2}$ at energies $\varepsilon_\nu \sim$ 1.5-15 TeV, and inferred luminosity $\varepsilon_\nu dL_{\nu_\mu}/d\varepsilon_\nu \sim 3 \times 10^{42}$ erg/s in this range. Meanwhile, upper limits for gamma rays above 0.2 TeV [16] rule out models in which TeV gamma rays and neutrinos escape the source

with similar flux. Some recent proposals invoke proton acceleration and neutrino production in hot coronal regions near the BH where X-rays are emitted via thermal Comptonization, either accretion disk coronae [18, 19] or accretion shocks [20, 21], so that accompanying gamma rays would be significantly absorbed via $\gamma\gamma$ interactions with AGN photons.

Here we propose an alternative picture where protons are accelerated in the inner regions of the wind relatively near the BH in NGC 1068, which has various advantages over the coronal region models. DSA, a well established mechanism for particle acceleration, is assumed. This region may be identified with a "failed" wind that is plausibly expected in radiative, line-driven wind models for the conditions corresponding to NGC 1068 [22]. Neutrinos are mainly generated via pp and $p\gamma$ interactions with the AGN radiation, while $\gamma\gamma$ interactions mediate the associated pair cascade emission, which we evaluate across the full EM spectrum. For the GeV gamma rays, we invoke a separate region where the wind interacts with the torus, accelerates protons via DSA and induces pp interactions with the torus gas. This allows GeV photons to escape, while TeV photons are $\gamma\gamma$-absorbed by IR photons from the torus. All relevant emission processes are modeled self-consistently with a detailed numerical code. More details can be found in Ref. [1].

2. Model Formulation

DSA at collisionless shock waves with sufficiently high Mach numbers can convey a sizable fraction of the energy of bulk plasma motion into that of non-thermal particles [6]. In the inner regions of AGN winds near the BH, shocks may naturally form [23] in failed winds that are robustly expected in models of line-driven winds from the accretion disk, particularly for the BH mass $M_{\rm BH}$ and $\lambda_{\rm Edd}$ inferred for NGC 1068 [22]. Such flows are initially launched from the inner parts of the disk (typically at radii $R \lesssim 100R_s$, where $R_s = 2GM_{\rm BH}/c^2$ is the Schwarzschild radius), but do not exceed the escape velocity $v_{\rm esc} = (2GM_{\rm BH}/R)^{1/2}$ due to overionization and eventually fall back, thereby interacting with gas flowing out subsequently. Henceforth we assume that protons are accelerated by DSA in the inner regions of the wind, with the total proton power L_p as a parameter. At the same time, a successful wind exceeding $v_{\rm esc}$ can be line-driven from the outer parts of the disk, mainly in the equatorial direction that is shielded from ionization. This outer wind can propagate farther and impact the torus [17] potentially inducing strong shocks and DSA of protons, for which we assume a total proton power $L_{p,o}$. The model geometry is illustrated in Fig.1 of [1].

Employing a numerical code that builds on previous work [24, 25], we model the multi-messenger (MM) emission induced by a population of high-energy protons interacting with magnetic fields, radiation and/or gas. For either the inner region of the failed wind or the outer region of the wind-torus interaction, the emission region is a uniform, stationary sphere of radius R_x with a tangled magnetic field of amplitude B_x, through which all charged particles are advected with the bulk flow velocity v_x. The index x is denoted o for the outer region, while it is dropped when referring to the inner region.

The inner region is permeated by radiation from the AGN that are the dominant targets for $p\gamma$ and $\gamma\gamma$ interactions as well as seed photons for inverse Compton (IC) processes. Adopting $D = 14$ Mpc, its spectrum is of a standard, geometrically thin accretion disk around a BH with $M_{\rm BH} = 3\times10^7 M_\odot$ peaking in the optical-UV at $\varepsilon_{\rm disk} \simeq 32$ eV with total luminosity $L_{\rm disk} \simeq L_{\rm bol} = 10^{45}$ erg/s (implying $\lambda_{\rm Edd} \simeq 0.27$), plus an X-ray emitting corona with photon index $\Gamma_{\rm cor} = 2$,

exponential cutoff energy $\varepsilon_{\rm cor} = 128\,$keV and 2-10 keV luminosity $L_{\rm cor,2-10} = 7\times10^{43}\,$erg/s [13], adopting parameters consistent with observations of NGC 1068 (Fig.2). See Ref. [1] for more details.

For the inner region, we assume $v = v_{\rm esc}(R)$, as expected for failed winds. In steady state, the bulk of the plasma should escape the region via advection on a dynamical timescale $t_{\rm dyn} = R/v$, either from the polar regions toward the BH, or from the equatorial regions toward the accretion disk. The average gas density n can be related to R and L_p as follows. As the average pre-shock velocity of particles is $v \sim v_{\rm esc}$, the total pre-shock kinetic energy in the inner region is of order $E_k \sim (1/2)m_p n v^2 (4\pi/3)R^3 = (2\pi m_p/3) n R^3 v^2$. If a fraction $f_{\rm CR}$ of this is channelled into protons, $f_{\rm CR}E_k \sim L_p t_{\rm dyn}$, so that $n = 3L_p t_{\rm dyn}/2\pi m_p f_{\rm CR} R^3 v^2 = 3L_p/2\pi m_p f_{\rm CR} R^2 v^3$.

The outer region is the part of the torus that interacts strongly with the outer wind, mostly where the latter grazes the torus funnel, rather than near the disk where gas must be inflowing [17]. It contains gas with average density n_o as pp targets, and is also immersed in thermal radiation that serve mainly as $\gamma\gamma$ targets, emitted from the inner torus of radius $R_{\rm tor} = 0.1\,{\rm pc} \gtrsim R_o$ and temperature $T_{\rm tor} = 1000\,$K, as constrained by near IR observations of NGC 1068 [17]. We also set $v_o = 5000\,$km/s for physical consistency with an outer, successful wind in scenarios of line-driven winds [22].

For each region, protons are injected with total power $L_{p,x}$ and a power-law distribution in energy, $dN_p/dE_p \propto E_p^{-2}$, from $E_{p,\rm min} = m_p c^2$ up to an exponential cutoff characterized by $E_{p,{\rm max},x}$ Subsequent pp and/or $p\gamma$ (photomeson and photopair or Bethe-Heitler; BeH) interactions lead to production of secondary hadrons, leptons and photons, of which charged pions and muons decay into neutrinos. Photons with sufficient energy trigger pair cascades via $\gamma\gamma$ interactions. The charged particles generate photons by synchrotron and IC processes. The steady state distribution of all particles and the resulting MM emission are obtained self-consistently by solving the coupled kinetic equations that account for their radiative losses and advective escape. As $v_x < c$, Doppler effects are weak, and the emission is quasi-isotropic.

The value of $E_{p,{\rm max},x}$ is set where DSA is limited by the available time or radiative losses, $t_{{\rm acc},x}(E_p) = \min[t_{{\rm dyn},x}, t_{{\rm rad},x}(E_p)]$, where $t_{{\rm acc},x}(E_p) = (10/3)(c\eta_{g,x}E_p/eB_x v_x^2)$ is the DSA timescale and $\eta_{g,x} \gtrsim 1$ parameterizes the strength of magnetic turbulence, $t_{{\rm dyn},x} = R_x/v_x$, and $t_{{\rm rad},x}(E_p)$ is the radiative loss timescale, primarily pp, photopion and BeH losses for the inner region, $t_{\rm rad} = (t_{pp}^{-1} + t_{p\gamma\pi}^{-1} + t_{\rm BeH}^{-1})^{-1}$, and pp loss for the outer region, $t_{{\rm rad},o} = t_{pp}$.

The main parameters are R, B, η_g, L_p for the inner region and R_o, n_o, B_o, $L_{p,o}$ for the outer region. These are adjusted to best describe the MM data, also considering physical plausibility. We posit $f_{\rm CR} = 0.2$, a reasonable value for DSA. For B, $B^2/8\pi = \epsilon_B(1/2)m_p n v^2$ (or $B = (6\epsilon_B L_p/f_{\rm CR} r^2 v)^{1/2}$) with $\epsilon_B \lesssim 0.5$ delineates a plausible range.

3. Results

Analytic estimates of the relevant timescales and neutrino spectra are discussed at length in Ref. [1]. Numerical calculations generally confirm our analytic estimates for the neutrinos, and also allow detailed studies of the broadband EM emission caused by complex hadronic cascade processes. We fiducially adopt for the inner region $R = 30R_s \simeq 2.7\times10^{14}\,$cm, $L_p = 10^{44}\,$erg/s. $B = 154\,$G ($\epsilon_B = 0.5$), and $\eta_g = 10^3$. These parameters imply $E_{p,\rm max} \simeq 150\,$TeV and $n = 1.2\times10^{10}\,{\rm cm}^{-3}$.

For the outer region, we choose $R_o = 0.1$ pc and $n_o = 10^6\,\mathrm{cm}^{-3}$, and adjust B_o and $L_{p,o}$ to be consistent with the EM data.

Fig.1 compares the physically relevant timescales for the inner region in the fiducial case: the dynamical timescale $t_{\rm dyn}$, the acceleration timescale $t_{\rm acc}$, and radiative loss timescales due to pp t_{pp}, photopion $t_{p\gamma\pi}$, Bethe-Heitler $t_{\rm BeH}$, and proton synchrotron $t_{\rm psyn}$. Comparison among these determines the value of $E_{p,\rm max}$. The observed steep neutrino spectrum necessitates $\eta_g \gg 1$. Such values for η_g are also commonly inferred for electron acceleration in blazars [26].

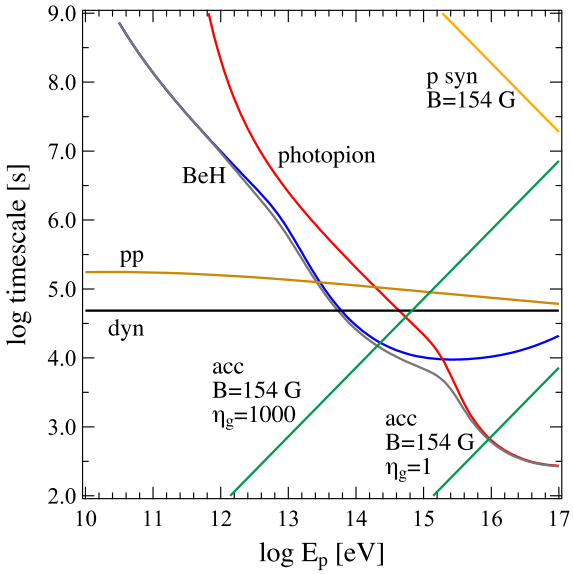

Figure 1: Comparison of timescales for the inner region in the fiducial case. Dynamical time $t_{\rm dyn}$ (black), pp loss time (brown), photopion loss time $t_{p\gamma\pi}$ (red), Bethe-Heitler loss time $t_{\rm BeH}$ (blue), total photohadronic loss time (gray), proton synchrotron loss time $t_{\rm psyn}$ (ochre) for $B = 154\,\mathrm{G}$ ($\epsilon_B = 0.5$), acceleration time $t_{\rm acc}$ (green) for $\{B = 154\,\mathrm{G}, \eta_g = 1\}$ and $\{B = 154\,\mathrm{G}, \eta_g = 10^3\}$.

Fig.2 presents the fiducial numerical results compared with the available MM data for NGC 1068. Neutrinos from the inner region are predominantly due to pp but also contain a non-negligible $p\gamma$ component, with spectral cutoffs at $\varepsilon_{\nu,\rm max} \sim 5$ TeV, generally consistent with the current IceCube data. Also present is a sub-dominant pp neutrino contribution from the outer region.

EM emission from the inner region is dominated by the pp cascade. Despite considerable $\gamma\gamma$ attenuation above a few MeV as expected, it is luminous enough to contribute significantly to the observed sub-GeV emission, mostly via IC upscattering of AGN photons by first-generation pp cascade pairs. At higher energies, pp gamma rays from the outer region take over, where $L_{p,o} = 1.3 \times 10^{42}\,\mathrm{erg/s}$. Above ~0.1 TeV, the pp gamma rays are severely $\gamma\gamma$-attenuated by the torus IR radiation, in agreement with the current upper limits.

The cascade emission from the inner region extends down to the radio-far IR bands and may contribute to the sub-mm emission detected by ALMA on sub-pc scales [21], although the spectral slope below a few 100 GHz is flatter than observed due to synchrotron self absorption. (However, accounting for the broader sub-mm emission may still be feasible by considering a suitable radial distribution of physical properties, beyond our one zone model.) Also observationally relevant may be GHz-band synchrotron emission from the outer region by secondary pairs from pp-induced $\pi^\pm$

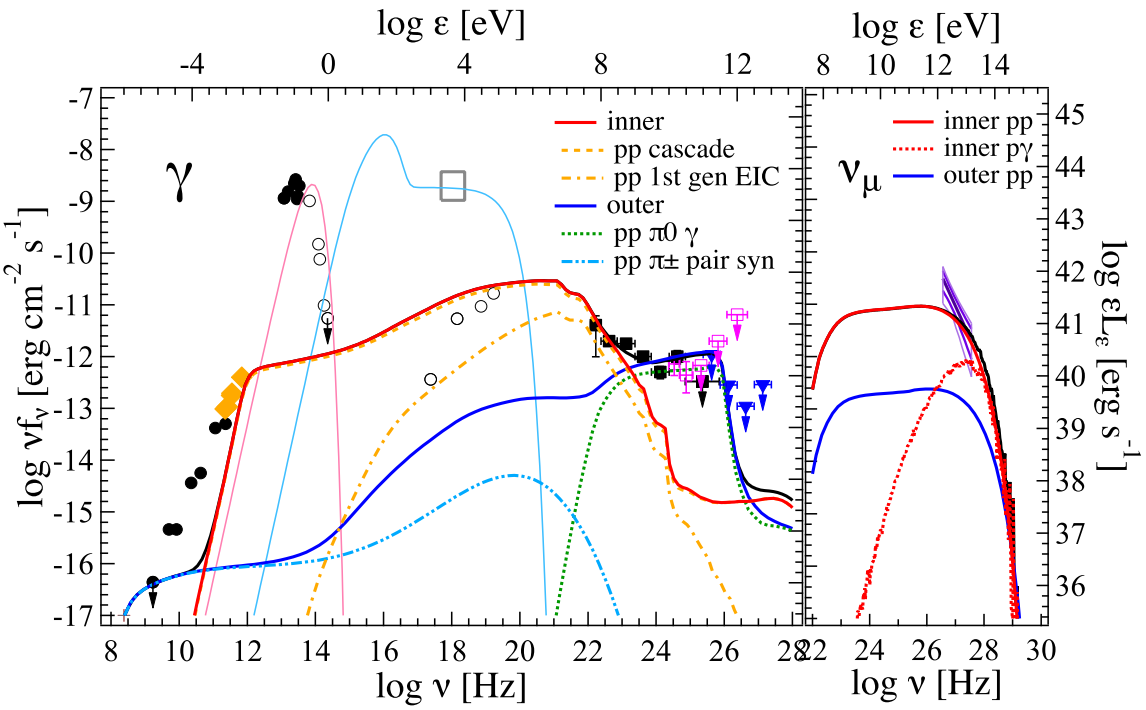

Figure 2: Model vs. observations of the multi-messenger spectrum of NGC 1068 for fiducial parameters. Inner region: $R = 30R_s$, $B = 154\,\mathrm{G}$ ($\epsilon_B = 0.5$), $\eta_g = 1000$, $L_p = 10^{44}$erg/s. Outer region: $R_o = 0.1\,\mathrm{pc}$, $n_o = 10^6\,\mathrm{cm}^{-3}$, $B_o = 15\,\mathrm{mG}$, $L_{p,o} = 1.3 \times 10^{42}\,\mathrm{erg/s}$. Total emission from the inner (red solid), outer (blue solid), and both (black solid) regions shown. Left: Electromagnetic spectrum. Components dominating each band highlighted: total pp cascade (ochre dashed), external inverse Compton (EIC) from first-generation pp cascade pairs (ochre dot-dashed), pp π^0 decay (green dotted), pp $\pi^\pm$ decay pair synchrotron (cyan double-dot-dashed). Assumed disk+corona (cyan thin) and torus (magenta thin) components overlaid. Data plotted for radio to X-rays on sub-pc scales (black circles) [27], distingushing bands affected by obscuration (empty circles), high resolution ALMA (ochre diamonds) [21], Fermi-LAT (black and magenta squares) [28, 29] and MAGIC (blue triangles) [16]. Intrinsic X-ray flux (gray box) indicated [13]. Right: Muon neutrino spectrum. Best fit line (thick), 1- (medium) and 2- (light) σ error regions from IceCube denoted [12].

decay. (Note that the general origin of radio emission in radio-quiet AGN is under debate, one possibility being non-thermal emission from AGN winds [7].) For consistency with the current upper limit at a few GHz, we choose $B_o = 15\,\mathrm{mG}$, within the range inferred from independent polarization measurements for the inner torus of NGC 1068 [30]. This implies $E_{p,\mathrm{max},o} = 600$ TeV, set by $t_{\mathrm{acc},o} = t_{\mathrm{dyn,o}}$ if $\eta_{g,o} = 10$.

4. Discussion

The principal assumption here for the inner region is that near the BH at $R \lesssim 100R_s$, protons are accelerated on a timescale $\gtrsim r_g c/v^2 = cE_p/eBv^2$ with total power $L_p \sim 0.1L_{\mathrm{bol}}$, and undergo pp and $p\gamma$ interactions with ambient protons and photons on a timescale $\sim R/v$. Plausibly accounting for the neutrinos observed from NGC 1068 entails $v \sim v_{\mathrm{esc}}$. We identify this with regions of failed winds that are robustly expected in line-driven models of AGN winds.

Although shocks in failed, line-driven winds are seen in numerical simulations [23], they are yet to be analyzed in detail. Failed winds have been proposed to be the origin of some other known features of AGN, such as dense X-ray obscurers near the nucleus (possibly present in NGC 1068), part of the broad line region, and the soft X-ray excess [22, 31]. Further studies, both theoretical and observational, are warranted to clarify the existence and properties of failed winds in AGN, and how they compare with the current model. For the outer region, future work should account for the clumpy structure of the torus, synchrotron and IC emission from primary electrons, as well as an underlying starburst contribution.

Similar to the coronal region models [18–21], the prominent MeV-GeV cascade emission (Fig.2) may be decipherable with current GeV and/or future MeV-GeV instruments for NGC 1068 and other nearby AGN. As the sub-GeV emission, and possibly also the sub-mm emission, arises from $\lesssim 100R_s$, variability is expected on timescales down to hours, albeit with limited amplitude due to the weak Doppler effects. MM variability correlations between neutrinos, sub-GeV, sub-mm and/or optical emission on longer timescales caused by variations in the mass accretion rate $\dot{M}$ provide a potential test. The $\gamma\gamma$ origin of the TeV gamma-ray break can be tested with CTA [33].

Although detailed discussions are beyond the current scope, we may speculate on expectations of this model for AGN other than NGC 1068. In coronal region models, the neutrino luminosity would correlate with the X-ray luminosity, and the fact that NGC 1068 is the brightest AGN for IceCube is attributed to its intrinsic X-ray brightness [18, 21], combined with its favorable declination for the detector [19]. In the current wind model, an additional factor may be high $\lambda_{\rm Edd}$, required for high wind power [22, 32] (also valid e.g. for the Circinus galaxy). The extent of the region of failed winds may depend systematically on $\lambda_{\rm Edd}$, $M_{\rm BH}$ and the UV-X-ray spectra of AGN [22]. This implies important differences from other models for the neutrino and cascade EM emission of different AGN, as well as the diffuse neutrino background from all AGN, to be explored in the future.

Most intriguingly, neutrinos and gamma rays may be unique probes of the inner regions of AGN where winds are launched from the accretion disk and interact with their immediate environment, especially in obscured objects. Future high-energy MM observations may provide important new insight into the physics of AGN winds, which are widely believed to play a critical role in the evolution of supermassive BHs and galaxies.

References

[1] S. Inoue, M. Cerruti, K. Murase, R.-Y. Liu, *PRL* submitted. [arXiv:2207.02097].

[2] R. Blandford, D. Meier, A. Readhead, *ARA&A* **57** (2019) 467.

[3] S. Veilleux, R. Maiolino, A. D. Bolatto, S. Aalto, *A&Ap. Rev.* **28** (2020) 2.

[4] S. Laha, C. S. Reynolds, J. Reeves, G. Kriss, M. Guainazzi, R. Smith, S. Veilleux, D. Proga, *Nat. Ast.* **5** (2021) 13.

[5] C. M. Harrison, T. Costa, C. N. Tadhunter, A. Flütsch, D. Kakkad, M. Perna, G. Vietri, *Nat. Ast.* **2** (2021) 198.

[6] A. R. Bell, *Astropart. Phys.* **43** (2013) 56.

[7] F. Panessa, R. D. Baldi, A. Laor, P. Padovani, E. Behar, I. McHardy, *Nat. Ast.* **3** (2019) 387.

[8] C.-A. Faucher-Giguère, E. Quataert, *MNRAS* **425** (2012) 605.

[9] R.-Y. Liu, K. Murase, S. Inoue, C. Ge, X.-Y. Wang, *ApJ* **858** (2018) 9.

[10] C. Ramos Almeida, C. Ricci, *Nat. Ast.* **1** (2017) 679.

[11] M. Ackermann et al., *ApJ* **755** (2012) 164.

[12] IceCube Collaboration, *Science* **378** (2022) 538.

[13] A. Marinucci et al., *MNRAS* **456** (2016) L94.

[14] T. M. Yoast-Hull, J. S. Gallagher, E. G. Zweibel, J. E. Everett, *ApJ* **780** (2014) 137.

[15] B. Eichmann, J. Becker Tjus, *ApJ* **821** (2016) 87.

[16] V. A. Acciari et al., *ApJ* **883** (2019) 135.

[17] S. García-Burillo, F. Combes, C. Ramos Almeida, et al., *A&A* **632** (2019) A61.

[18] K. Murase, S. S. Kimura, P. Mészáros, *PRL* **125** (2020) 011101.

[19] A. Kheirandish, K. Murase, S. S. Kimura, *ApJ* **922** (2021) 45.

[20] Y. Inoue, D. Khangulyan, S. Inoue, A. Doi, *ApJ* **880** (2019) 40.

[21] Y. Inoue, D. Khangulyan, A. Doi, *ApJ* **891** (2020) L33.

[22] M. Giustini, D. Proga, *A&A* **630** (2019) A94.

[23] S. A. Sim, D. Proga, L. Miller, et al., *MNRAS* **408** (2010) 1396.

[24] M. Cerruti, A. Zech, C, Boisson, S. Inoue, *MNRAS* **448** (2015) 910. [arXiv:1411.5968].

[25] M. Cerruti, M. Kreter, M. Petropoulou, A. Rudolph, F. Oikonomou et al., PoS(ICRC2021)979.

[26] S. Inoue, F. Takahara, *ApJ* **463** (1996) 555.

[27] M. A. Prieto, J. Reunanen, K. R. W. Tristram et al., *MNRAS* **402** (2010) 724.

[28] M. Ajello et al., *ApJS* **232** (2017) 18.

[29] S. Abdollahi et al., *ApJS* **247** (2020) 33.

[30] E. Lopez-Rodriguez, C. Packham, T. J. Jones et al., *MNRAS* **452** (2015) 1902.

[31] M. Giustini, D. Proga, [arXiv:2202.07564].

[32] M. Nomura, K. Ohsuga, C. Done, *MNRAS* **494** (2020) 3616.

[33] CTA Consortium, [arXiv:1709.07997].